



Research Article

Exploring a Mallorca cave flooding during the Little Ice Age using nondestructive techniques on a stalagmite: micro-CT and XRF core scanning

Mercè Cisneros^{1,2} , Isabel Cacho¹, Jaime Frigola¹, Ana Moreno³, Heather Stoll⁴, Joan J. Fornós⁵ , Javier Sigró² and Mariano Barriendos⁶

¹GRC Geociències Marines, Departament de Dinàmica de la Terra i de l'Oceà, Facultat de Ciències de la Terra, Universitat de Barcelona, c/ Martí i Franqués s/n, 08028 Barcelona, Spain; ²Centre en Canvi Climàtic, Departament de Geografia, Facultat de Turisme i Geografia, Universitat Rovira i Virgili, c/ Joanot Martorell 15, 43480, Vila-seca, Tarragona, Spain; ³Departamento de Procesos Geoambientales y Cambio Global, Instituto Pirenaico de Ecología-CSIC, Av. Montañana 1005, 50059, Zaragoza, Spain; ⁴Departamento de Geología, Universidad de Oviedo, c/ Jesús Arias de Velasco s/n, 33005, Oviedo, Spain; and Department of Earth Sciences, ETH Zürich, Clausiusstrasse 25, 8092, Zurich, Switzerland; ⁵Grup de Recerca en Ciències de la Terra, Universitat de les Illes Balears, ctra/ de Valldemossa, 07122, Mallorca, Spain and ⁶IDAEA, Instituto de Diagnóstico Ambiental y Estudios del Agua, Consejo Superior de Investigaciones Científicas, c/ Jordi Girona 18-26, 08034 Barcelona, Spain

Abstract

This study focuses on characterizing a discontinuity within the Seán stalagmite (4.75–7.75 cm) by means of two nondestructive techniques: (1) high-resolution micro-computed tomography (micro-CT) and (2) X-ray fluorescence (XRF) core scanning (XRFCS). Micro-CT was used to study the stalagmite density, and XRFCS was applied to obtain the qualitative elemental composition and colour measurements. The new data obtained from nondestructive techniques have been combined with previously published geochemical data and fabric determinations from the same stalagmite found in Sa Balma des Quartó cave in Mallorca. The two methodologies applied in the present study have improved the characterization of the distinctive horizon. The micro-CT images identified the layer as a minor event due to the high air content. The distinctive horizon is characterized by a high Ti-content, indicating the arrival of terrigenous particles. Based on those observations, together with the fact that the micrite layer appears filling the gaps between the older columnar fabric, we argue that the micrite layer may represent a major flooding event inside the cave after the year 1616 ± 23 CE and before the year 1623 ± 28 CE, which can be related to an extreme rainfall event. This hypothesis is further supported by the observed cave flooding during the autumn of 2018.

Keywords: Speleothems, Paleohydrology, Hydrometeorological extreme events, Cave floodings, Micro-CT, XRF core scanning, Central-western Mediterranean Sea, Little Ice Age (LIA)

(Received 28 December 2022; accepted 28 August 2023)

INTRODUCTION

The Mediterranean region is considered to be highly vulnerable to global warming (Giorgi, 2006). It is considered a hot spot in terms of future climate change scenarios outlined by climate models, with expected drastic hydrological changes, such as intense precipitation events and extreme periods of drought (Gibelin and Deque, 2003; Giorgi, 2006; Ulbrich et al., 2006; Giorgi and Lionello, 2008; Sheffield and Wood, 2008; Mariotti et al., 2008; Drobinsky et al., 2020). Although the total annual precipitation in the Balearic region is decreasing, the contribution of minimum and maximum daily precipitation (in respect to the average: up to 4 mm and above 64 mm, respectively) to the yearly total is increasing (Homar et al., 2010). During the last few decades, intense rain events in the

western Mediterranean Basin have caused numerous catastrophic floods in several countries, with human casualties (Pastor et al., 2001), like those during autumn 2018 in Mallorca Island (Grimalt-Gelabert et al., 2020, 2021). Studying past extreme events can be useful in dealing with the coming challenges as consequences of global warming. Considering the climate sensitivity of this region, numerous studies based on speleothems have reconstructed the climate of different periods in the past (Hodge, 2004; Hodge et al., 2008; Dumitru et al., 2018; Torner et al., 2019; Cisneros et al., 2021) as well as past sea levels (Vesica et al., 2001; Polyak et al., 2018; Dumitru et al., 2019).

During the Little Ice Age (LIA; 1275 to 1850 CE in Cisneros et al. [2016]), frequent extreme rain events have been described in previous global studies. For instance, some of these extreme events in the western Mediterranean region were: an increase in the runoff in the Alboran Sea (Nieto-Moreno et al., 2011) and in the central-western part (Margaritelli et al., 2018); humid episodes in the northern part (Bassetti et al., 2016); predominant wet conditions in the Iberian Peninsula and northern Morocco

Corresponding author: Mercè Cisneros; Email: mercecisneros@gmail.com

Cite this article: Cisneros M, Cacho I, Frigola J, Moreno A, Stoll H, Fornós JJ, Sigró J, Barriendos M (2023). Exploring a Mallorca cave flooding during the Little Ice Age using nondestructive techniques on a stalagmite: micro-CT and XRF core scanning. *Quaternary Research* 1–13. <https://doi.org/10.1017/qua.2023.52>

© The Author(s), 2023. Published by Cambridge University Press on behalf of Quaternary Research Center. This is an Open Access article, distributed under the terms of the Creative Commons Attribution licence (<http://creativecommons.org/licenses/by/4.0/>), which permits unrestricted re-use, distribution and reproduction, provided the original article is properly cited.



coincident with frequent North Atlantic Oscillation (NAO) phases (Ait Brahim et al., 2018; Ramos-Román et al., 2018); the most important flood of the last millennium in the Ebro River basin (Balasch et al., 2019); increased lake levels in southern Spain (Martín-Puertas et al., 2010); and flood event enhancement in the Iberian Peninsula (Barriendos and Martín-Vide, 1998; Benito et al., 2003; Moreno et al., 2008; Barriendos et al., 2019). The general LIA climate variability has been attributed to repeated volcanic eruptions in a short time (Crowley, 2000; Robock, 2000; Bertler et al., 2011; Miller et al., 2012; McGregor et al., 2015), solar minima (Bard et al., 2000; Mayewski et al., 2006; Ammann et al., 2007), and changes in the thermohaline circulation (Broecker, 2000, 2001; Lund et al., 2006).

Regarding the techniques used in this study, micro-computed tomography (micro-CT) and X-ray fluorescence (XRF) core scanning (henceforth XRFCS) allow rapid, continuous, nondestructive, repetitive, and high-resolution analyses of sedimentary sequences (Frigola et al., 2015). Consequently, these techniques are very valuable techniques in earth science research (Mees et al., 2003). Micro-CT is a 3D imaging and analysis method to investigate internal structures of a large variety of objects, including geomaterials (Cnudde and Boone, 2013). XRFCS allows analysis of the qualitative elemental composition for elements between aluminium and uranium with resolutions up to 100 μm (Jansen et al., 1998; Rothwell and Rack, 2006). This technique is widely applied in geosciences studies to better characterize the sources of and processes responsible for the final deposits (Moreno et al., 2004; Morellón et al., 2011; Nieto-Moreno et al., 2011; Rodrigo-Gámiz et al., 2011; Frigola et al., 2015; Cisneros et al., 2016; Torner et al., 2019; Cerdà-Domènech et al., 2020).

In reference to the application of both techniques to speleothems, the number of studies is scarce but growing, particularly in recent years. Since the pioneering work of Mickler et al. (2004), which explored the potential of micro-CT to determine the growth axis, this technique has been applied in speleothems with diverse objectives: studying 3D textures of speleothems, like those that develop inside historic walls (Martínez-Martínez et al., 2010); exploring the potential of the stalagmite for fluid-inclusion analyses (Zisu et al., 2012); obtaining paleoclimate proxies in unsectioned stalagmites (Walczak et al., 2015); characterizing petrological features (Vanghi et al., 2015); and explaining U-Th outliers (Bajo et al., 2016). The XRFCS technique has been applied in speleothems for reconstructing variations in atmospheric sulphate (Frisia et al., 2005), paleoclimate and paleoenvironmental changes (Dandurand et al., 2011; Martínez-Pillado et al., 2020), volcanic eruptions (Badertscher et al., 2014), and paleoflood events in caves (Finné et al., 2015; Denniston and Luetscher, 2017) and as a tool for speleothem trace element analysis (Vansteenberghe et al., 2020).

Speleothems have also been used as proxies for extreme rainfall or other hydrologic drivers of cave flooding (Gázquez et al., 2014; González-Lemos et al., 2015; Denniston and Luetscher, 2017). For instance, elevated Ti data (obtained by XRFCS) compared with the calcite matrix in speleothems have been used to identify paleofloods events in southern Greece (Finné et al., 2015). In addition, previous studies have traced cave floods in the form of detrital layers recorded in stalagmites (Borsato et al., 2003; Dorale et al., 2005; Dasgupta et al., 2010).

In the present study, the micro-CT and XRFCS techniques are coupled to explore a discontinuity in the studied speleothem (Seán stalagmite, Sa Balma des Quartó cave, Mallorca). After combining the results with geochemical data and fabric observations of the stalagmite previously published in Cisneros et al.

(2021), we present here the first description of a cave flooding event based on a speleothem from the central-western Mediterranean region.

CAVE AND CLIMATIC SETTINGS

The Seán stalagmite was recovered from Sa Balma des Quartó cave, located in the southeastern part of Mallorca in the Balearic Islands (see Fig. 1a and b). The cavity is formed in upper Miocene reef limestone (Ginés et al., 2014) and is located near a cliff that reaches a maximum height of 20 m, running parallel to the coast. The Miocene calcarenites are rich in marine microfossils. The length of the cave is 70 m and consists basically of a wide chamber formed by collapse (Fig. 1c and d), characterized by a rich decoration of speleothems (Bermejo et al., 2014). The bottom of the chamber is 12.5 m from the surface and 10.5 m above sea level. The access to the cave consists of a small vertical hole in the outside rock shelter. According to the monitoring results (Cisneros et al., 2021), the cave annual ventilation begins to be enhanced by the end of autumn. During winter and spring is when the cave is more ventilated. At present, the surrounding area consists of a forest formed by Mediterranean vegetation (species like *Quercus ilex*, *Pistacia lentiscus*, or genus *Juniperus*; Bolós, 1996), which is rather undisturbed by human activities.

Sa Balma des Quartó cave is dominated by seepage flow (Cisneros et al., 2021). Despite that, evidence of episodic water flows has been observed in one side of the cave after the extreme rain event that occurred during autumn 2018 in Mallorca Island (Grimalt-Gelabert et al., 2021, 2020; Fig. 2).

Climate in Balearic Islands corresponds to a typical Mediterranean pattern, being characterized by mild, wet winters and warm to hot, dry summers (Lionello et al., 2006). The maximum rainfall occurs during the autumn and decreases during the winter and spring, with a very dry summer season. In Mallorca Island, present-day rainfall is characterized by high irregularity, with alternation of dry and wet years, and is affected by intense precipitation events related to cyclogenetic Mediterranean conditions and the geographic trends of the island (the precipitation in the northern mountains is usually higher than in the southern zones; Grimalt-Gelabert et al., 2020). Heavy rainstorms, which can occasionally produce 400 mm of rain in 24 hours, are typical and affect mainly the mountainous area in the northwestern part of the island, as well as on the east coast (Grimalt and Rosselló, 2018), where the studied cave is located (Fig. 1b).

The rainfall distribution on the western Mediterranean region has been associated with atmospheric circulation patterns as the NAO. Positive NAO modes cause stronger winter storms crossing the Atlantic on a more northerly track, reducing the transport of humidity over the Mediterranean and enhancing the evaporation-precipitation balance (Tsimplis and Josey, 2001; Lionello and Sanna, 2005).

MATERIAL AND METHODS

This study aims to characterize a discontinuity in the Seán stalagmite by means of two nondestructive techniques: (1) high-resolution micro-CT and (2) XRFCS. Micro-CT was applied in a section of the Seán stalagmite (4.75–7.75 cm) where the discontinuity was observed and where a thin section had been previously performed. XRFCS was used in the same section to obtain the qualitative elemental composition and colour measurements by means of a high-resolution colour line-scan camera.

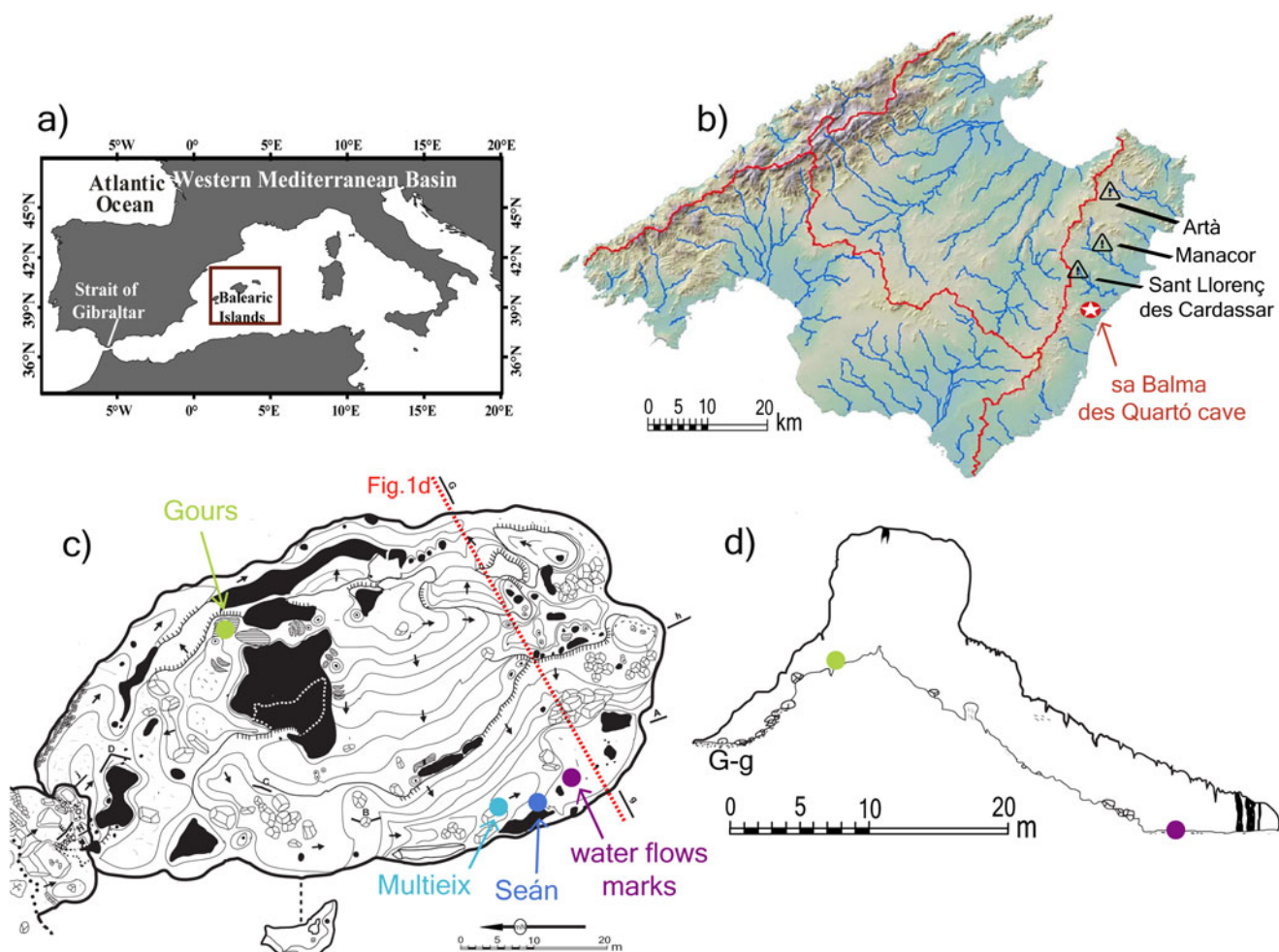


Figure 1. Studied area. (a) Map of the western Mediterranean showing Balearic Islands, where Mallorca is located. (b) Distribution of the superficial hydrology of Mallorca Island; streams are indicated in blue and watersheds in red (adapted from Grimalt-Gelabert et al., 2020). Location of Sa Balma des Quartó cave is indicated as well as the municipalities most affected by the severe flood that occurred on October 9, 2018 (Grimalt-Gelabert et al., 2021). (c) Topography of Sa Balma des Quartó cave (Bermejo et al., 2014). Position of the vertical profile in part d is also indicated. Blue circles correspond to the location of the speleothems recovered in situ. (d) Vertical profile ("G-g" section in Bermejo et al., 2014). Filled circles in c and d represent sites where evidence of cave flooding was observed after the extreme rain event of October 2018.

The data derived from the nondestructive techniques, which are presented for the first time in this study, are combined with geochemical data ($\delta^{18}\text{O}$, $\delta^{13}\text{C}$, trace element ratios, and U/Th dates) and fabric observations performed on the Seán stalagmite and published in Cisneros et al. (2021). A second stalagmite from the same cave, named Multeix (Cisneros et al., 2021), is taken into account at some points of the discussion, as it overlaps with the Seán stalagmite.

Seán stalagmite and previous data

The Seán stalagmite was found broken in the lower part of Sa Balma des Quartó cave (Fig. 1). Before analysis, the stalagmite was cut into two halves, and the fabric and the discontinuities along the axial length were determined using optical microscopy of thin sections (Cisneros et al., 2021).

The internal microstratigraphy of the Seán stalagmite (approx. 12×5 cm) was characterized following the methodology and the nomenclature proposed by Martín-Chivelet et al. (2017). Seán has a regular and flat external surface and a cylindrical shape and presents a white and translucent surface along the growth

axis (Fig. 3). It has been divided in two unconformity-bounded units (UBUs): UBU2 from the base to 6.00 cm and UBU1 from 6.00 cm to the top. In a general way, the morphostratigraphic units could be described as flat-topped with well-defined and sub-horizontal growth layers, and aggradational stacking pattern sets (Muñoz-García et al., 2016) are generalized along this stalagmite. Most of the speleothem is characterized by columnar calcite fabrics and a remarkable and uniform lamination (<1 mm) along the growth axis. For a more detailed characterization of the entire stalagmite, refer to the supplementary material in Cisneros et al. (2021).

The age of the Seán stalagmite is based on U-Th dating of nine samples, published in Cisneros et al. (2021; Table 1) and performed according to the procedures of Edwards et al. (1987). Ages were obtained with a Neptune Thermo Finnigan Multi-Collector ICP-MS at the University of Minnesota (USA). Ages are corrected taking into account an initial $^{230}\text{Th}/^{232}\text{Th}$ atomic ratio of $(4.4 \pm 2.2) \times 10^{-6}$ (Cheng et al., 2013).

The age model was produced using the R statistics package Bchron (Parnell et al., 2008). It was performed in two sections to minimize uncertainties: from the bottom to the unconformity



Figure 2. Pictures of evidence of flood into Sa Balma des Quartó cave in November 2018: (a and b) in the upper part of the cave, gours containing water (blue lines); (c) in the lower part of the cave, marks of water flows (purple lines).

at 6.00 cm and from there to the top. One U-Th age was excluded to minimize the outlier probability in the adjacent dates (Cisneros et al., 2021).

The lower and upper boundaries of the age uncertainties, according to all the age models obtained by Bchron, have statistically the same significance (95%). The results show that Seán grew quite continuously between 1421 CE and 1880 CE with a mean growth rate of 0.4 mm/yr (from 0.1 to 0.9 mm/yr).

UBU1 and UBU2 are separated by a brown millimetric layer ca. 6.00 cm that seems to correspond to a detrital or allogenic horizon. At 6.00 cm from the top, this millimetric brown layer shows micrite fabric, and above this layer, some isolated mosaic fabrics have been also observed. Around 6.00 cm, skeletal components have been also distinguished, which could correspond to a gastropod of 1400 μm length. (Fig. 4). Although the brown layer follows the general lamination pattern, its thickness varies

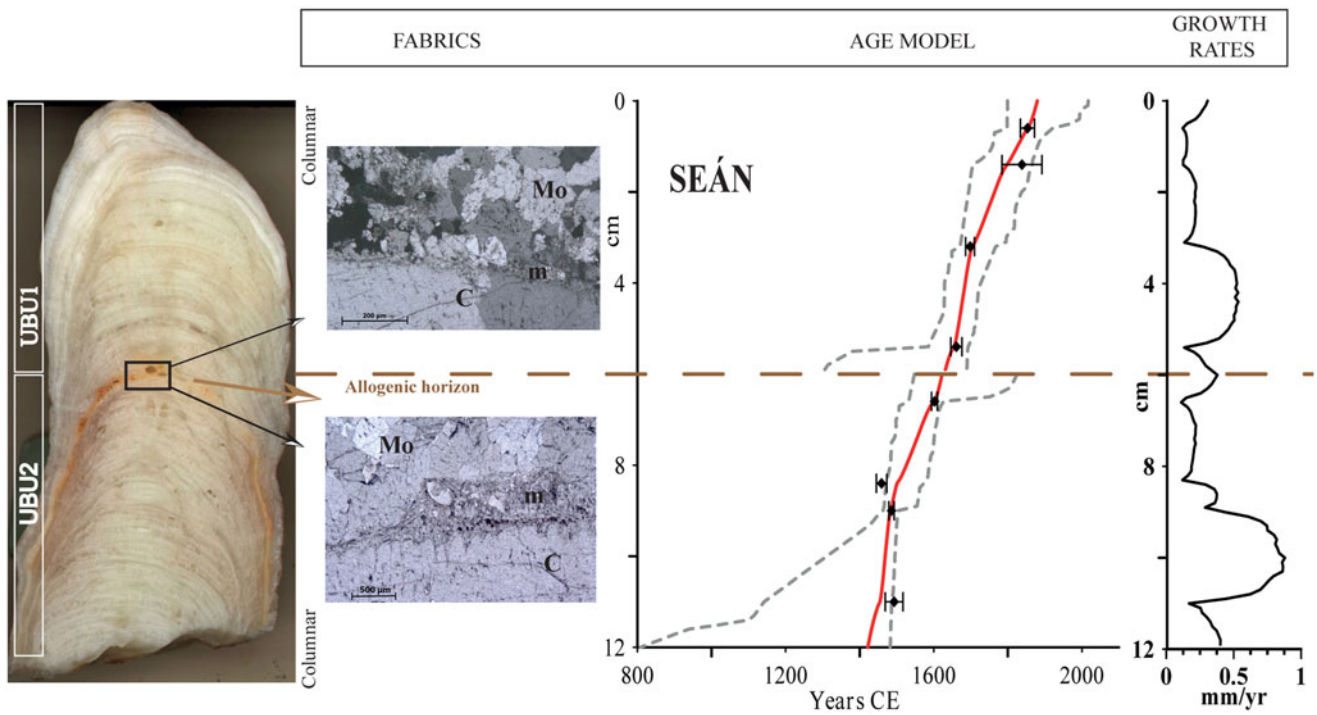


Figure 3. Synthesized description of the Seán stalagmite (from Cisneros et al., 2021). The brown dashed line indicates the layer/unconformity ca. 6.00 cm. Shown in relation to the fabric pictures are those around 6.00 cm (from top to bottom): top, isolated mosaic fabrics (Mo) above the micrite layer (m), columnar fabric below (C), cross-polarized light; bottom, columnar (C), mosaic (Mo), and micrite (m) fabrics, plane-polarized light. U-Th age model performed on Bchron. Red plots are the final age models. Black diamonds represent the U-Th ages (2σ error). Grey dashed lines correspond to the total range of ages covered by all the age models obtained with Bchron, which have statistically the same significance (95% per; confidence interval).

Table 1. Summary of the results of U-Th analyses used in the age model of the Seán stalagmite (2σ error) and published in Cisneros et al. (2021).

Sample distance from the top (cm) of Seán stalagmite	Year		
	(corrected) ^a		
0.6	1852.9	±	18.8
1.4	1837.9	±	53.9
3.2	1697.9	±	11.8
5.4	1660.6	±	15.1
6.6	1602.4	±	7.7
8.4	1459.1	±	13.5
9	1486.0	±	6.6
10	924.7	±	29.0
11	1493.0	±	23.6

^aAge in italics is not included in the age model. All years are CE.

between 1.3 and 2.5 mm. The thickness of the detrital horizon is 0.25 mm (located between 6.25 and 6.00 cm). According to the age model (Cisneros et al., 2021), the distinctive horizon was accumulated after 1616 ± 23 CE (6.25 cm) and before 1623 ± 28 CE (6.00 cm). Because the growth rates around the micrite layer were similar to the average growth rates obtained from the UBU2 part, the previous study concluded that no significant erosion took place (Cisneros et al., 2021; Fig. 3).

Stable isotopes and trace element samples were manually microdrilled at 1 mm intervals along the growth axis. Although $\delta^{18}\text{O}$ data in the centimetres around the brown layer are similar to the mean values of the entire stalagmite record (from 4.7 to -4.9 ‰), $\delta^{18}\text{O}$ values right along the detrital horizon tend to be more depleted (Cisneros et al., 2021). $\delta^{13}\text{C}$ values just before the beginning of the layer are enriched considering the rest of the record (6.25 cm, -6.50 ‰), and values tend to be more depleted along the layer (-8.2 ‰). In reference to trace elements (Mg/Ca, Sr/Ca, and Ba/Ca), the values of the ratios present fluctuations during the detrital horizon, and the general trend is to decrease (from 7.33 to 5.47, from 0.13 to 0.083, from 0.009 to 0.006, respectively).

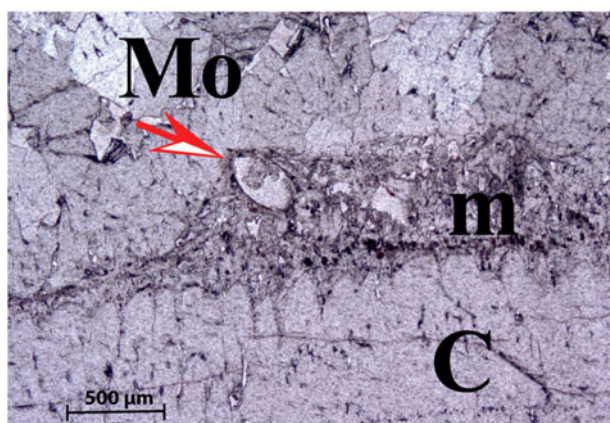


Figure 4. Fabric picture of the Seán stalagmite thin section ca. 6.00 cm. Columnar (C), mosaic (Mo), and micrite (m) fabrics, plane-polarized light. The arrow indicates the gastropod test.

To gain a better understanding of the event that affected the cave and caused the brown layer in Seán, a second stalagmite from the same cave has been included in the “Discussion.” This stalagmite, named Multieix, was found ~ 5 m distant from where the Seán stalagmite was lying (Fig. 1c). The particular morphology and length of this stalagmite, which presents three different growth axes, has been also observed in remaining active stalagmites in a specific site within the cave, just where it was found. This suggests that it was recovered near its growth position, although its base was not identified. Considering all of this, Multieix’s growth position is located approximately 2 m higher than the Seán site. The Multieix stalagmite is 30.5 cm in length and grew from the year 302 BCE to 1844 CE. Only its top 5 cm grew up simultaneously with Seán (during the 1503–1844 CE period). No new data for the Multieix stalagmite are presented in this study; more detailed information can be found in Cisneros et al. (2021).

Micro-CT scanning

The density of the stalagmite has been studied in Seán ca. 6.00 cm (~ 4.75 – 7.75 cm) using micro-CT scanning with a Multitom CORE X-ray CT system in the CORELAB, University of Barcelona. The scanner was operated at a tube voltage of 140 kV and an intensity of 33 W. The exposure time was 800 ms, the voxel size was 33 μm , and the number of projections was 1500. Reconstructed images of the relative density values were exported as 16-bit images using the AVIZO (FEI) software. This technique allows obtaining slices with voxel resolution ranging from 5 to 300 μm (Frigola et al., 2015). The micro-CT scanning results are expressed in this study as 2D images in a colour map scale denoting relative density values.

XRFCS

The qualitative elemental composition of the Seán stalagmite was studied between ~ 4.75 and 7.75 cm from the top, corresponding to the same segment used for micro-CT analyses, with an Avaatech XRF core-scanner system (CORELAB, University of Barcelona). The scanning resolution was 200 μm , and the measured window was adjusted to 8 mm to align with the laminae of the stalagmite. Analyses were focused on the left part of the growing axis. Elements with atomic weights between aluminium and iron were analysed at 10 kV, 1.95 mA, and a 60 s exposure time, while elements with atomic weights between iron and lead were analysed at 30 kV, 1.95 mA, and a 90 s exposure time.

The colour measurements were conducted along the left side of the growth axis of the entire Seán stalagmite. A high-resolution (70 micron pixels) visible image of the Seán stalagmite was obtained with a colour line-scan camera mounted in the Avaatech XRFCS System. The acquisition software provides images in several formats and also numerical colour values in RGB and CIE-Lab coordinates at the same high resolution. Visible pictures do not require any additional treatment, as is shown in Figure 3. The $L^*a^*b^*$ values (colour coordinates) are at the scale of uniform colour defined by the Commission Internationale de l’Eclairage (CIE; Muñoz et al., 2015). L^* corresponds to lightness and ranged in value from 0 (black) to 100 (white). The proxies a^* and b^* represent variations between red-green and yellow-blue, respectively, ranging in values between -120 and 120 (Westland, 2012). Colour coordinates enable recognition of changes in the carbonate content, as well as the presence

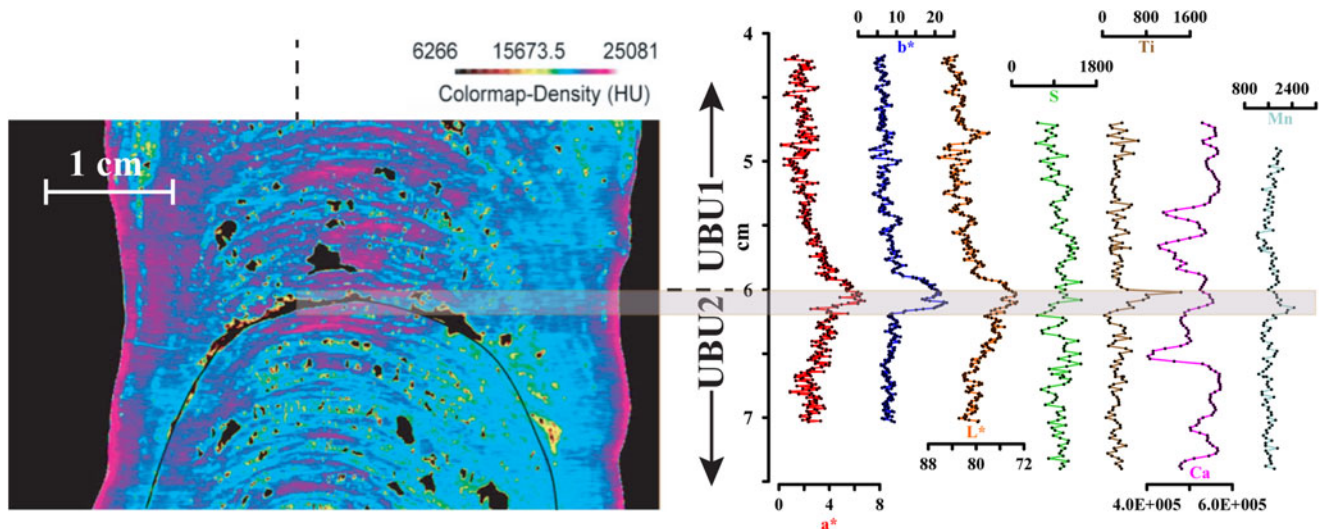


Figure 5. Micro-computed tomography (micro-CT) and X-ray fluorescence (XRF) core scanning (XRFCS) results (this study) from the boundary of the two unconformity-bounded units (UBUs) in Seán (4.75–7.75 cm). Left, Colour map from micro-CT between (HU, Hounsfield units); horizontal grey bar indicates the detrital layer (from 6.00 cm to 6.25 cm). Right panel (from left to right), Coordinates of colour CIE $L^*a^*b^*$; S, Ti, Ca, and Mn elements (expressed as peak area). XRFCS measurements were carried out on the left part of the growth axis of the stalagmite. Vertical and discontinuous black line (above the left image) indicates the line of measurements.

of iron and clays (Mix et al., 1992; Nederbragt and Thurow, 2004; Rogerson et al., 2006; Debret et al., 2011).

RESULTS

Micro-CT scanning

Micro-CT scanning provides a density colour map that reveals certain differences in the analysed section at around 6.00 cm of the Seán stalagmite (Fig. 5, left panel). Along the growth axis, a continuous lamination has been observed, consisting of dense laminae (25,081–15,673.5 Hounsfield units [HU]) alternating with more porous laminae (15,673.5–6266 HU).

Colour-map densities < 6266 HU correspond to air measurements, and the 15,673.5 HU value to dispersions of the X-ray beam due to the edge effect. The brown lamina at ca. 6.00 cm presents high air content (~6266 HU), and below this lamina, certain lineal structures are observed, which are not present in UBU1. The 2D images point out a high air content in the brown layer across the entire stalagmite and not only in the surface of the split stalagmite. Thus, in agreement with Vanghi et al. (2015), micro-CT has improved the characterization of the speleothem, providing information about spatial distribution of porosity and stratigraphic architecture.

XRFCS results

Colour measurements and qualitative elemental composition results obtained for the boundary between the two UBUs of Seán at ca. 6.00 cm are shown in Figure 5. Colour measurements ($L^*a^*b^*$ values for colour coordinates) obtained from the high-resolution pictures define an abrupt change in the boundary between both UBUs of Seán (ca. 6.00 cm). Parameters b^* (yellow-blue) and L^* (lightness) indicate more differences in the boundary than parameter a^* (red-green). The three parameters increase their values along the brown layer starting at 6.25 cm until 5.90 cm.

Regarding XRFCS results, where S, Ti, Mn, and Ca profiles are expressed as peak areas (Fig. 5), the examined section displays

significant oscillations in the analysed elements. All of these elements exhibit a certain enhancement beginning around 6.50 cm. S values decrease around 6.75 cm and increase around 6.00 cm. The S record shows several oscillations but without any significant change associated with the UBU limit. Ti shows an abrupt enhancement from 6.20 cm until 6.00 cm ($\sim 1617 \pm 25$ CE to 1623 ± 28 CE), reaching the maximum values at 6.00 cm. In the Mn profile, a remarkably rapid increase occurs at ca. 4.70 cm (1671 ± 13 CE), and the lowest values were obtained at 5.60 cm (1642 ± 26 CE). This element also shows a relative enhancement at ca. 6.00 cm. With regard to Ca, maxima values occurred at 6.80 cm (1585 ± 16 CE), and around 6.00 cm, this element shows a relatively less abrupt increase than the other elements presented here. At the beginning of the brown layer (6.25 cm), Ca values are low ($\sim 480,000$ peak area) and tend to decrease and, later, to be enhanced until 6.00 cm ($\sim 554,000$ peak area).

DISCUSSION

Interpretation of the allogenic or detrital horizon: sediment sources and causes

The micrite layer at ca. 6.00 cm marks the limit between the two described UBUs of the Seán stalagmite (Fig. 5). This layer is associated with a significant Ti peak and is also accompanied by abrupt changes in the colour parameters, according to the results obtained by the XRFCS (Fig. 5). The brown layer follows the general lamination according to micro-CT scanning results; no important signs of erosion or hiatuses in the deposition have been detected; and thus, Seán apparently grew quite continuously. Although a microhiatus cannot be absolutely disregarded, this unconformity consists of a minor event that does not seem to be responding to longer-term variations in drip rates or drastic changes in the growth rates.

In the study by Finné et al. (2015) in southern Greece, elevated Ti (obtained by XRFCS) compared with the calcite matrix has been used to identify paleoflood events. In the Seán stalagmite,

the presence of high Ti values and also of a micrite layer suggests the enhanced arrival of terrigenous particles, corresponding to an allogenic or detrital horizon.

In this study, among the potential sources of this distinctive layer, the influence of a large volcanic eruption was initially considered, because such events have frequently been attributed to the dominant cold temperatures of the LIA (Crowley, 2000; Robock, 2000; Bertler et al., 2011; Miller et al., 2012; McGregor et al., 2015). Nevertheless, this layer is not related to any sulphur (S) peak or $\delta^{13}\text{C}$ enrichment in the Seán stalagmite (Fig. 6d and f), both of which are typically detected in records associated with volcanic eruptions at other locations (Frisia et al., 2008; Badertscher et al., 2014). In addition, according to the global and Northern Hemisphere volcanic eruptions recorded by Gao et al. (2008) and Crowley and Unterman (2012) for the last centuries, the period coincident with this distinctive layer of the Seán stalagmite is not characterized by the most severe eruptions recorded (Fig. 6l).

One mechanism capable of transporting the material of the distinctive layer to our cave, which is interpreted according to the significant Ti peak obtained by means of the XRFCS in the brown layer (Fig. 6g), is the supply of dust aerosols. Numerous studies have demonstrated the influence of Saharan dust in our study area (Goudie and Middleton, 2001; Moreno et al., 2002) and its contribution to the red Mediterranean soils (Muhs et al., 2010). In addition, Saharan dust has been detected in cave soil sediments in Mallorca (Fornós et al., 2009) and in stalagmites from the eastern Mediterranean through Sr and U isotopes (Frumkin and Stein, 2004). Saharan dust is mostly supplied by wet deposition (“muddy rain”), when the air mass becomes fresh after being in contact with the sea, while dry deposition only takes place occasionally (Fiol et al., 2005).

The period during which the distinctive horizon was accumulated according to the age model (1616 ± 23 CE to 1623 ± 28 CE) is coincident with a drop in sea-surface temperature (SST) considering the available multidecadal timescale reconstruction derived from marine sediments recovered in the study area (Cisneros et al., 2016; Fig. 6j). The years of the distinctive horizon have been characterized by positive and negative NAO phases (Fig. 6k), according to the multiannual reconstruction of Faust et al. (2016). If the $\delta^{18}\text{O}$ record is interpreted as hydroclimate variability (Cisneros et al., 2021), the values obtained for the period corresponding to the brown layer, which are similar to the mean values of the entire stalagmite record, do not indicate years that were especially wet or dry or that experienced extreme rain or drought events (Fig. 6e). Hence, it is not feasible to determine whether this episode corresponds to a deposition of dry or wet dust.

In agreement with previous studies, the distinctive layer and the Ti peak detected in the Seán stalagmite could be interpreted as a cave flood tracer (Borsato et al., 2003; Dorale et al., 2005; Dasgupta et al., 2010; Finné et al., 2015) and/or as a proxy for extreme rainfall or other hydrologic drivers of cave flooding (Gázquez et al., 2014; Denniston and Luetscher, 2017).

Although Sa Balma des Quartó cave is dominated by seepage flow (Cisneros et al., 2021) and has been described as a very dry cave in the present day, evidence of episodic water flows has been observed in one side of the cave during October 2018 after an extreme rain event that may have led to the inundation of the base of the cave (Figs. 1d and 2). An inundation like that one occurring in the past could easily have covered the 6.00 cm of Seán studied here, which would be the length of the stalagmite at the moment of the flooding (Fig. 7). The hypothesis of the cave

flooding agrees with the fact that the micrite layer fills the gaps between the older columnar fabric (Fig. 4).

When considering the distinctive layer of the Seán stalagmite as an allogenic or detrital horizon, distinction between an absolute external source of the sediment (allogenic material) or absolute in situ fine sediments mobilized by water (detrital material) cannot be established. However, the presence of the gastropod in the distinctive layer of the stalagmite (Fig. 4) likely points to the mobilisation by water of the in situ sediments. The Miocene calcarenites of the karst system are rich in these marine microfossils, which could arrive in suspension to the stalagmite and be fixed by the next calcite growth. The arrival of the gastropod to the surface of the stalagmite via drip water or by falling down from the limestone of the cave ceiling cannot be excluded.

Present and past cave floodings and extreme rain events

On October 9, 2018, an extreme rain event occurred in Mallorca, resulting in a severe flood due to the high intensity and amount of precipitation. The flood took place on the eastern coastline of the island, affecting the municipalities of Sant Llorenç des Cardassar, Artà, and to a lesser extent, Capdepera and Manacor, and was the most severe flood occurring in Sant Llorenç in the last 80 yr (Grimalt-Gelabert et al., 2021; Fig. 1b). The amount of rainfall in Sant Llorenç during October 9, 2018, was 257 mm, and the effects were severe: nine lives were lost, several bridges and infrastructures collapsed, and numerous vehicles were dragged (Grimalt-Gelabert et al., 2020, 2021). Several weeks later, on 16 November, we visited Sa Balma des Quartó cave and found clear evidence of cave flooding as a consequence of the extreme event. The group of gours in the upper part of the cave were full of water for the first time in the 5 yr of monitoring (Fig. 2), and water flow tracks were observed in the cave sediments of the lower part of the cave (Figs. 1d and 2). Typically, Sa Balma des Quartó cave has been described as a very dry cave in the present day, and the gours of the upper part of the cave have been described as being empty of water (Bermejo et al., 2014). Regarding the floor of the lower part of the cave, it is covered by sediments and acts like a sediment sink (Bermejo et al., 2014); observation of flow tracks in the sediments have not been frequent during the last years.

These observations inside the cave indicate a response associated with extreme rainfall events and reinforce the hypothesis that the micrite layer of the Seán stalagmite can be interpreted as a result of past cave flooding, which occurred after 1616 ± 23 CE (6.25 cm) and before 1623 ± 28 CE (6.00 cm). The cave was possibly flooded by an extreme rain event, with enough water to cover the 6.00 cm length of the Seán stalagmite. The water could flow over the detrital sediments deposited earlier in the cave, supplying these sediments to the stalagmite surface (Fig. 7). Nevertheless, it cannot be discarded that the water inflow could introduce sediments from the external surface into the cave. It should be noted that the length of the Seán stalagmite regarding the current position of the cave floor could possibly be different from today due to the sediments supplied by the inflow water.

The calcite growth previous to the micrite layer shows columnar fabrics and micro-CT scanning results that point out significant high relative density values ($>15,673.5$ HU), as was expected to find associated with this kind of fabric (Vanghi et al., 2015; Fig. 5). Columnar fabrics have usually been related to constant drip rates (Frisia, 2015) that in some way could be associated with rather constant climatic conditions. These conditions could

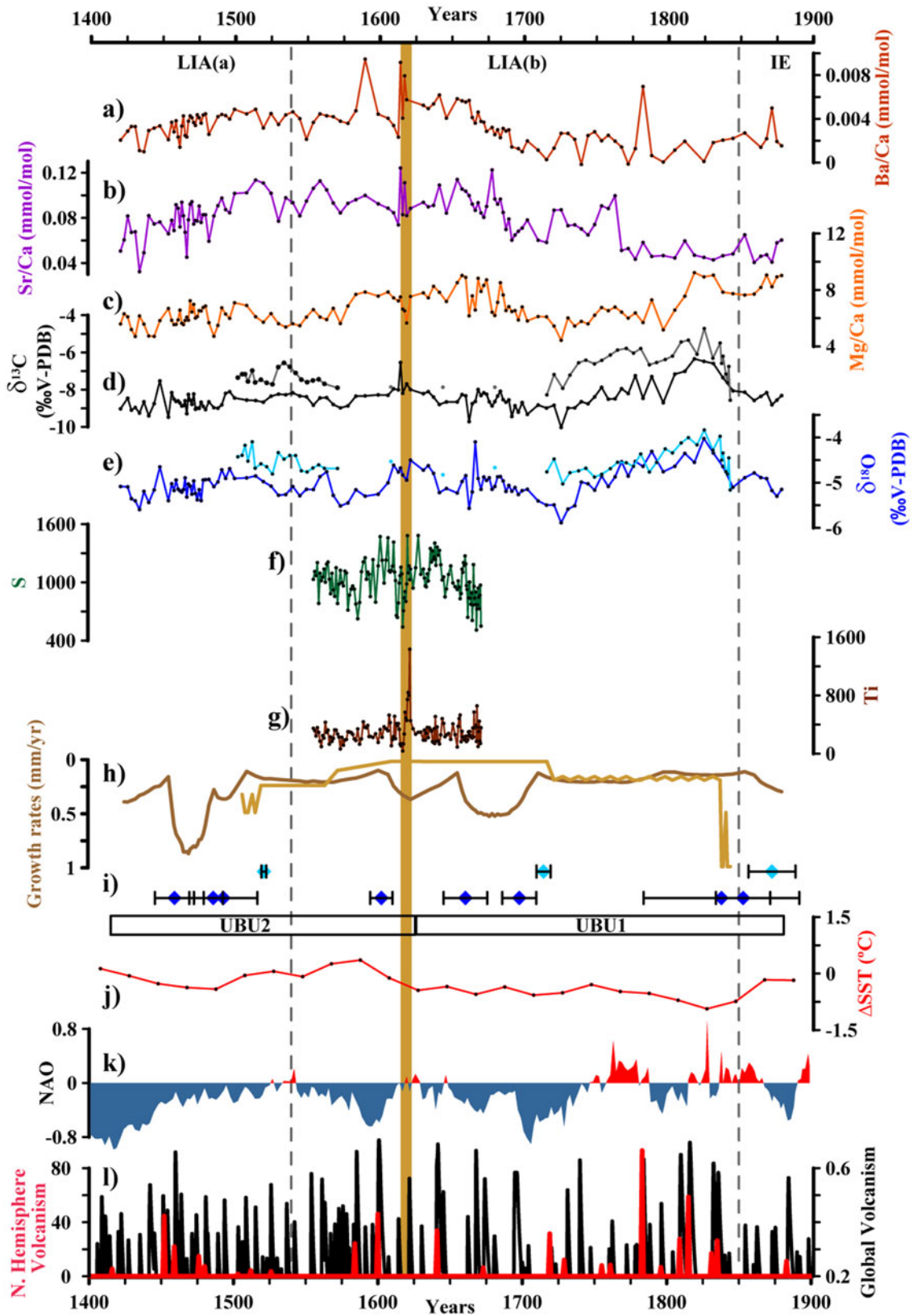


Figure 6. Results presented in this study from the Seán stalagmite compared with previously published data for the Seán and Multiex stalagmites, North Atlantic Oscillation (NAO) reconstruction and volcanism activity. (a–e) Ba/Ca, Sr/Ca, Mg/Ca, $\delta^{13}\text{C}$, and $\delta^{18}\text{O}$ records for the Seán stalagmite. $\delta^{13}\text{C}$, $\delta^{18}\text{O}$ records from Multiex are also shown in lighter colours (Cisneros et al., 2021). (f and g) S and Ti from X-ray fluorescence (XRF) core scanning (XRFCs) analyses (this study). (h and i) Growth rates and U/Th ages (diamonds) of Seán and Multiex stalagmites (Cisneros et al., 2021). (j) Mg/Ca sea-surface temperature (SST) from north Minorca (Cisneros et al., 2016). (k) NAO reconstruction (Faust et al., 2016). (l) Northern and global volcanism (Gao et al., 2008; Crowley and Unterman, 2012). Both sub-periods of Little Ice Age (LIAa and LIAb) and the Industrial Era (IE) are also indicated. Brown vertical band indicates discontinuity and brown layer observed in Seán (~6.00 cm), which corresponds to the limit between both unconformity-bounded units (UBUs) in the Seán stalagmite.

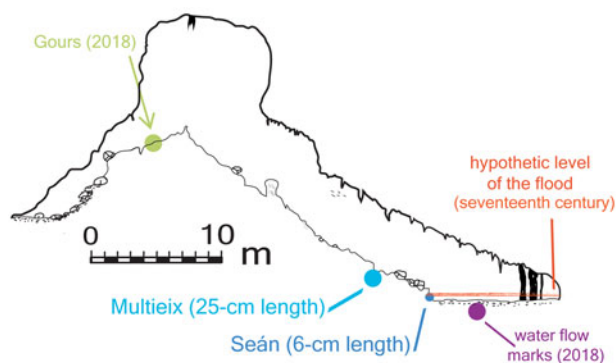


Figure 7. Hypothetical reconstruction of the cave flooding during the seventeenth century. Topography corresponds to the vertical profile of Sa Balma des Quartó cave (“G-g” section in Bermejo et al., 2014) also shown in Fig. 1d. Blue circles correspond to the locations where the speleothems were found, which are separated by a distance of ~5 m. Seán’s growth position is located approximately 2 m lower than the Multieix site. The hypothetical flood level, which is represented in qualitative terms, would have covered the 6.00 cm length of the Seán stalagmite in that moment. The evidence of cave flooding observed after the extreme rain event of October 2018 (gours with water in the upper part and water flow marks in the lower part) is also indicated.

be interpreted to be predominant during a few years before 1615 ± 23 CE.

The micrite layer presents a high air content according to the micro-CT data and a significant abrupt Ti increase, as well as a slight enhancement of Mn and Ca, according to the XRFCS data. In this micrite layer, $\delta^{18}\text{O}$ values tend to be more depleted and the values of the trace element ratios tend to decrease (Fig. 6a–e). The more depleted $\delta^{18}\text{O}$ values could indicate a reduction of the evaporation due the contact of the stalagmite surface with the water flow as a consequence of the cave flood. Regarding the decreasing trend of Mg/Ca ratio (Fig. 6c), the relative enhancement of Ca detected by XRFCS analyses along the detrital horizon should be noted (until 6.00 cm; 1623 ± 28 CE; Fig. 5). Despite this relative Ca enhancement along the detrital horizon, Ca values tend to decrease at the beginning of the brown layer. Previous studies have recorded reduced Ca peak areas in clay horizons (Finné et al., 2015).

Concerning the contact time between the “muddy” water and the stalagmite surface, we can only assert that the posterior calcite growth, according to the age model, had already precipitated ca. 1623 ± 28 CE (~6 yr later). It should be noted that: (1) the two U/Th age uncertainties obtained close to the detrital horizon at ca. 6.00 cm (5.4 cm, 1660 ± 15 CE; and 6.600 cm, 1602 ± 8 CE) are really low, and (2) growth rates around the micrite layer are similar to the mean obtained in the UBU2 of the Seán stalagmite (Cisneros et al., 2021; Fig. 6h and i). The time during which no layers of clean calcite (without detrital material) precipitated could indicate that the water inflow volume supplied by the rainfall was severe (Fig. 7). It should be noted that after the extreme rain event of October 2018, only a few centimetres of water were found in the gours of the upper part of the cave weeks later (Fig. 2a and b). Thus, the extreme rain that occurred in 2018 was possibly less severe than the past event of the seventeenth century, as it covered the 6.00 cm length of the Seán stalagmite (Fig. 7).

Mosaic fabrics have been observed after the micrite layer of the Seán stalagmite (Cisneros et al., 2021). This kind of fabric has been reported as a product of dissolution of columnar calcite and re-precipitation of mosaic calcite driven by an influx of

undersaturated waters causing dissolution of a preexisting fabric (Frisia, 2015). The presence of isolated crystals in mosaic after the micrite layer could possibly be associated with new contacts (occasional and/or intermittent) between the muddy water and the stalagmite surface. We consider the occurrence of the contacts as occasional and/or intermittent, because no important hiatus was detected in the record. Moreover, based on the minor event indicated by micro-CT images and fabric observations, the unconformity of the Seán stalagmite does not appear to align with significant shifts in growth rates or prolonged fluctuations in drip rates.

After the cave flooding of 2018 and those that occurred during the seventeenth century, it is likely that the stagnant water gradually dissipated through infiltration into deeper levels within the karst. It should be noted that the coeval stalagmite, Multieix, does not present any evidence of allogenic or detrital sediments around these years. This stalagmite should have a length in that moment of ~25 cm and presents a very low growth rate (Fig. 6h). Multieix’s growth position is located approximately 5 m away from the Seán site but also ~2 m higher (Figs. 1c and 7). According to that, the probability that the water covered this stalagmite is much less than in the case of Seán. After the extreme rain event of 2018, no accumulated water or gours containing water were observed in the Multieix site.

The east of Mallorca, where Sa Balma de Quartó cave is located, shows the ideal conditions for episodes of heavy rain, in particular in situations of eastern cyclonic advection or Mediterranean depressions, as on the eastern coastline of the Iberian Peninsula (Grimalt-Gelabert et al., 2021). Previous studies based on historical documents have pointed out floods around Mallorca Island during the seventeenth century, particularly during the autumn of the years 1618, 1620, 1635, 1655, and 1683 (Campaner y Fuertes, 1881).

It should be noted that the most extreme rain event documented in the last 1000 yr occurred during November 1617 (Pino et al., 2018), when catastrophic floods have been described in more than 124 municipalities from the Mediterranean coast in the Iberian Peninsula, between Alacant and Perpignan. These floods caused general overflows and severe damage throughout the region, including the complete destruction of more than 445 infrastructures (Thorndycraft et al., 2006; Pino et al., 2018). In addition, the overflows of the Llobregat and Ter Rivers in Catalonia exceeded the magnitude of the events recorded for the last 3000 yr (Thorndycraft et al., 2006).

The fact that no more distinctive horizons have been detected during this period suggests the possibility of a very severe event recorded within the Seán stalagmite. While it is feasible to conduct more comprehensive research into the timing of the event, the intensity of the recorded event after 1616 ± 23 CE and before 1623 ± 28 CE likely aligns with the extreme rain event that took place in November 1617.

The micro-CT and XRFCS methodologies applied in this study have allowed a better characterization of the flood layer and its surroundings in the stalagmite and a better comprehension of the past flood event. The high relative density values (>15,673.5 HU) obtained by the micro-CT scanning in the calcite growth previous to the micrite layer (columnar fabrics) suggest that rather constant climatic conditions were predominant during a few years before 1615 ± 23 CE. Micro-CT results also indicated no important signs of erosion or hiatuses in the deposition of the Seán stalagmite, which apparently indicates continuous growth. In addition, the information provided by the 2D images and the

high air content (~6266 HU) obtained in the distinctive horizon pointed out that the event, which caused the lamina, affected entire width of the stalagmite and not only the surface of the split stalagmite. According to the XRFCS data, there was an abrupt enhancement of Ti between $\sim 1617 \pm 25$ CE and 1623 ± 28 CE (from 6.20 cm until 6.00 cm), confirming the enhanced arrival of terrigenous particles corresponding to the distinctive horizon.

CONCLUSIONS AND FUTURE PERSPECTIVES

In this study, we present new data of the characterization of a discontinuity in the Seán stalagmite using two nondestructive techniques: (1) high-resolution micro-CT and (2) XRFCS. Both techniques were applied to the 4.75–7.75 cm segment of the stalagmite. Micro-CT was used to study stalagmite density, while XRFCS was applied to obtain qualitative elemental composition and colour measurements by means of high-resolution colour line-scan camera. The results from these nondestructive techniques are combined with previous geochemical data ($\delta^{18}\text{O}$, $\delta^{13}\text{C}$, trace element ratios, and U/Th dates) and fabric observations published in Cisneros et al. (2021), which were performed in the same stalagmite from Sa Balma des Quartó cave in Mallorca.

The discontinuity in the Seán stalagmite was characterized in a previous study by Cisneros et al. (2021) as a millimetric brown layer with micrite fabric. Other observations included isolated mosaic fabrics above this layer, the presence of a gastropod, the layer filling gaps between older columnar fabric, and no significant difference in growth rates. The distinctive horizon was accumulated after 1616 ± 23 CE (6.25 cm) and before 1623 ± 28 CE (6.00 cm) and could correspond to an allogenic horizon.

The two methodologies applied in the present study have improved the characterization of the distinctive horizon. Mainly, they have provided information about spatial distribution of porosity and stratigraphic architecture (micro-CT) and qualitative composition of the layer (XRFCS), allowing a better understanding of its sediment sources and causes.

On the one hand, by means of the micro-CT scanning, the high relative density values ($>15,673.5$ HU) obtained below the micrite layer (columnar fabrics) suggest that rather constant climatic conditions were predominant during a few years before 1615 ± 23 CE. This technique also indicated no important signs of erosion or hiatuses in the deposition of the Seán stalagmite, which indicates that it grew continuously. In addition, the information provided by the 2D images and the high air content (~6266 HU) obtained in the distinctive horizon indicated that the event that caused the lamina affected the entire width of the stalagmite and not only the surface of the split stalagmite. This information, together with the fact that micrite is filling the older columnar fabrics, suggests a cave flood event as a cause of the distinctive horizon. On the other hand, according to the XRFCS data, an abrupt enhancement of Ti occurred between $\sim 1617 \pm 25$ CE and 1623 ± 28 CE (from 6.20 cm until 6.00 cm), which confirms the enhanced arrival of terrigenous particles, corresponding to the distinctive horizon. The terrigenous particles could correspond to an absolute external source of the sediment (allogenic material) or absolute in situ fine sediments mobilized by water (detrital material).

Although cave floodings in other regions have been identified by previous studies using detrital layers, this is the first time that such an event has been documented by an individual flood layer

in the studied area and period, representing an opportunity to use speleothems to describe past extreme events in the Mallorcan climate. The hypothesis of the cave flooding during the seventeenth century is reinforced by the observations in the cave response to the 2018 extreme rainfall that occurred in Mallorca.

A second stalagmite from the same cave, named Multieix, which overlaps with the Seán stalagmite (Cisneros et al., 2021), has been used to better understand the cave flooding in the past. The absence of any allogenic/detrital horizon in this stalagmite during the seventeenth century suggests that no sediment transported by water reached its location (which was 2 m higher than Seán and had a length of 25 cm at that time). Therefore, the flood did not extend to this elevated section of the cave.

Studies based on historical documents have pointed out floods around Mallorca Island during the seventeenth century, particularly during the autumn of the years 1618, 1620, 1635, 1655, and 1683 (Campaner y Fuertes, 1881). However, the most extreme rain event documented in the last 1000 yr occurred during November 1617 (Pino et al., 2018), when catastrophic floods have been described in more than 124 municipalities from the Mediterranean coast in the Iberian Peninsula, between Alacant and Perpignan.

The fact that no more distinctive horizons have been detected in the Seán stalagmite during this period probably suggests that the event recorded after 1616 ± 23 CE and before 1623 ± 28 CE could have been very severe. Although more detailed investigation about the moment of the flood can be developed, the severity of the event recorded by the Seán stalagmite possibly corresponds to the extreme rain event of November 1617.

Thus, the two nondestructive techniques (micro-CT and XRFCS) used in this study to characterize the discontinuity of the Seán stalagmite have allowed a better characterization of the detrital layer, which strongly suggests its causal relation with a flood. Micro-CT and XRFCS techniques hold significant potential for advancing our comprehension of the mechanisms responsible for discontinuities within a stalagmite, while preserving the integrity of the stalagmite itself. These techniques can complement the information derived from other data sources, such as fabric observations, thereby enhancing our understanding of the causes and sources of the sediment forming the distinct horizons within a stalagmite.

Acknowledgments. This work was funded by the projects TIMED (683237) of the European Research Council (Consolidator Grants); LACEN-CLI (2476-S/2017); OPERA (CTM2013-48639-C2-1-R); PLIOKAR (CGL2013-48441-P); CHIMERA (CTM2016-75411-R); PLIOKAR-II (CGL2016-79246-P, AEI-FEDER, EU); PLIOKAR-III (PID2020-112720GB-I00/AEI); SPYRIT (CGL2016-77479-R); and Generalitat de Catalunya, Grups de Recerca Consolidats (2017 SGR 315) to GRC Geociències Marines. We are grateful to M. Guart and T. Bullich for their collaboration in the laboratory tasks and to J. Ginés, À. Ginés, and A. Pilares for their collaboration in the fieldwork. MC benefits from a Margarita Salas postdoctoral fellowship at the University of Barcelona from the Ministerio de Universidades-Gobierno de España funded by European Union (NextGenerationEU funds). Many thanks are given to the editors, L. Piccini, and the anonymous reviewer for their constructive comments.

REFERENCES

- Ait Brahim, Y., Wassenburg, J.A., Cruz, F.W., Sifeddine, A., Scholz, D., Bouchaou, L., Dassi_e, E.P., Jochum, K.P., Edwards, R.L., Cheng, H., 2018. Multi-decadal to centennial hydroclimate variability and linkage to solar forcing in the Western Mediterranean during the last 1000 years. *Scientific Reports* 8, 17446.

- Ammann, C.M., Joos, F., Schimel, D.S., Otto-Bliesner, B.L., Tomas, R.A., 2007. Solar influence on climate during the past millennium: results from transient simulations with the NCAR climate system model. *Proceedings of the National Academy of Sciences USA* **104**, 3713–3718.
- Badertscher, S., Borsato, A., Frisia, S., Cheng, H., Edwards, R.L., Tüysüz, O., Fleitmann, D., 2014. Speleothems as sensitive recorders of volcanic eruptions—the Bronze Age Minoan eruption recorded in a stalagmite from Turkey. *Earth and Planetary Science Letters* **392**, 58–66.
- Bajo, P., Hellstrom, J., Frisia, S., Drysdale, R., Black, J., Woodhead, J., Borsato, A., et al., 2016. “Cryptic” diagenesis and its implications for speleothem geochronologies. *Quaternary Science Reviews* **148**, 17–28.
- Balasc, J.C., Pino, D., Ruiz-Bellet, J.L., Tuset, J., Barriendos, M., Castellort, X., Peña, J.C., 2019. The extreme floods in the Ebro River basin since 1600 CE. *Science of the Total Environment* **646**, 645–660.
- Bard, E., Raisbeck, G., Yiou, F., Jouzel, J., 2000. Solar irradiance during the last 1200 years based on cosmogenic nuclides. *Tellus B* **52**, 985–992.
- Barriendos, M., Gil-Guirado, S., Pino, D., Tuset, J., Pérez-Morales, A., Alberola, A., Costa, J., et al., 2019. Climatic and social factors behind the Spanish Mediterranean flood event chronologies from documentary sources (14th–20th centuries). *Global and Planetary Change* **182**, 102997.
- Barriendos, M., Martín-Vide, J., 1998. Secular climatic oscillations as indicated by catastrophic floods in the Spanish Mediterranean coastal area (14th–19th centuries). *Climatic Change* **38**, 473–491.
- Bassetti, M.A., Berné, S., Sicre, M.A., Dennielou, B., Alonso, Y., Buscail, R., Jalali, J., Hebert, B., Christophe Menniti, C., 2016. Holocene hydrological changes of the Rhone River (NW Mediterranean) as recorded in the marine mud belt. *Climate of the Past* **12**, 1539–1553.
- Benito, G., Sopena, A., Sánchez-Moya, Y., Machado, M.J., Pérez-González, A., 2003. Palaeoflood record of the Tagus River (central Spain) during the Late Pleistocene and Holocene. *Quaternary Science Reviews* **22**, 1737–1756.
- Bermejo, J., Mateu, T., López, B., Mingullón, R., Herráez, G., Villar, A., 2014. Cova de sa Balma des Quartó (Manacor, Mallorca). *Endins: publicació d'espeleologia*, no. **36**, 59–64.
- Bertler, N.A.N., Mayewski, P.A., Carter, L., 2011. Cold conditions in Antarctica during the Little Ice Age: implications for abrupt climate change mechanisms. *Earth and Planetary Science Letters* **308**, 41–51.
- Bolós, O. de, 1996. *La vegetació de les Illes Balears*. Institut d'Estudis Catalans, Barcelona, p. 269.
- Borsato, A., Quinif, Y., Bini, A., Dublyansky, Y., 2003. Open-system alpine speleothems: implications for U-series dating and paleoclimate reconstructions. *Studi Trentini di Scienze Naturali, Acta Geologica* **80**, 71–83.
- Broecker, W.S., 2000. Was a change in thermohaline circulation responsible for the Little Ice Age? *Proceedings of the National Academy of Sciences USA* **97**, 1339–1342.
- Broecker, W.S., 2001. Paleoclimate: was the medieval warm period global? *Science* **291**, 1497–1499.
- Campaner y Fuertes, A., 1881. *Cronicón Mayoricens*. J. Colomer y Salas, Palma.
- Cerdà-Domènech, M., Frigola, J., Sanchez-Vidal, A., Canals, M., 2020. Calibrating high resolution XRF core scanner data to obtain absolute metal concentrations in highly polluted marine deposits after two case studies off Portmán Bay and Barcelona, Spain. *Science of the Total Environment* **717**, 134778.
- Cheng, H., Edwards, L.R., Chou Shen, C., Polyak, V.J., Asmerom, Y., Woodhead, J., Hellstrom, J., et al., 2013. Improvements in ^{230}Th dating, ^{230}Th and ^{234}U half-life values, and U-Th isotopic measurements by multi-collector inductively coupled plasma mass spectrometry. *Earth and Planetary Science Letters* **371–372**, 82e91.
- Cisneros, M., Cacho, I., Frigola, J., Canals, M., Masqué, P., Martrat, B., Casado, M., et al., 2016. Sea surface temperature variability in the central-western Mediterranean Sea during the last 2700 years: a multi-proxy and multi-record approach. *Climate of the Past* **12**, 849e869.
- Cisneros, M., Cacho, I., Moreno, A., Stoll, H., Torner, J., Català, A., Edwards, R.L., Cheng, H., Fornós, J.J., 2021. Hydroclimate variability during the last 2700 years based on stalagmite multi-proxy records in the central-western Mediterranean. *Quaternary Science Reviews* **269**, 107137.
- Cnudde, V., Boone, M.N., 2013. High-resolution X-ray computed tomography in geosciences: a review of the current technology and applications. *Earth-Science Reviews* **123**, 1–17.
- Crowley, T.J., 2000. Causes of climate change over the past 1000 years. *Science* **289**, 270–277.
- Crowley, T.J., Unterman, M.B., 2012. Technical details concerning development of a 1200 yr proxy index for global volcanism. *Earth System Science Data* **5**, 187–197.
- Dandurand, G., Maire, R., Ortega, R., Devès, G., Lans, B., Morel, L., Perroux, A.S., et al., 2011. X-ray fluorescence microchemical analysis and autoradiography applied to cave deposits: speleothems, detrital rhythmites, and prehistoric paintings. *Géomorphologie: relief, processus, environnement, Groupe français de géomorphologie* **17**, 407–426.
- Dasgupta, S., Saar, M.O., Edwards, R.L., Shen, C.C., Cheng, H., Alexander, E.C., 2010. Three thousand years of extreme rainfall events recorded in stalagmites from Spring Valley Caverns, Minnesota. *Earth and Planetary Science Letters* **300**, 46–54.
- Debet, M., Sebag, D., Desmet, M., Balsam, W., Copard, Y., Mourier, B., Susperrigui, A.S., et al., 2011. Spectrocolorimetric interpretation of sedimentary dynamics: the new “Q7/4 diagram.” *Earth-Science Reviews* **109**, 1–19.
- Denniston, F., Luetscher, M.L., 2017. Speleothems as high-resolution paleoflood archives. *Quaternary Science Reviews* **170**, 1–13.
- Dorale, J.A., Lepley, S.W., Edwards, R.L., 2005. The ultimate flood recorder: flood deposited sediments preserved in stalagmites. *Geophysical Research Abstracts* **7**, 09901.
- Drobinsky, P., Da Silva, N., Bastin, S., Mailler, S., Muller, C., Ahrens, B., Christensen, O.B., Lionello, P., 2020. How warmer and drier will the Mediterranean region be at the end of the twenty-first century? *Regional Environmental Change* **20**, 78.
- Dumitru, O.A., Austermann, J., Polyak, V.J., Fornós, J.J., Asmerom, Y., Ginés, J., Ginés, J., Onac, B.P., 2019. Constraints on global mean sea level during Pliocene warmth. *Nature* **574**, 233–236.
- Dumitru, O.A., Onac, B.P., Polyak, V.J., Wynn, J.G., Asmerom, Y., Fornós, J.J., 2018. Climate variability in the western Mediterranean between 121 and 67 ka derived from a Mallorcan speleothem record. *Palaeogeography, Palaeoclimatology, Palaeoecology* **506**, 128–138.
- Edwards, R.L., Chen, J.H., Wasserburg, G.J., 1987. ^{238}U – ^{234}U – ^{230}Th – ^{232}Th systematics and the precise measurement of time over the past 500,000 years. *Earth and Planetary Science Letters* **81**, 175–192.
- Faust, J.C., Fabian, K., Milzer, G., Giraudeau, J., Knies, J., 2016. Norwegian fjord sediments reveal NAO related winter temperature and precipitation changes of the past 2800 years. *Earth and Planetary Science Letters* **435**, 84–93.
- Finné, M., Kylander, M., Boyd, M., Sundqvist, H.S., Löwemark, L., 2015. Can XRF scanning of speleothems be used as a non-destructive method to identify paleoflood events in caves? *International Journal of Speleology* **44**, 17–23.
- Fiol, L., Fornós, J.J., Gelabert, B., Guijarro, J.A., 2005. Dust rains in Mallorca (Western Mediterranean): their occurrence and role in some recent geological processes. *Catena* **63**, 64–84.
- Fornós, J.J., Ginés, J., Gràcia, F., 2009. Present-day sedimentary facies in the coastal karst caves of Mallorca island (western Mediterranean). *Journal of Cave and Karst Studies* **71**, 86–99.
- Frigola, J., Canals, M., Mata, P., 2015. Techniques for the non-destructive and continuous analysis of sediment cores. Application in the Iberian continental margin. *Boletín Geológico y Minero* **126**, 609–634.
- Frisia, S., 2015. Microstratigraphic logging of calcite fabrics in speleothems as tool for palaeoclimate studies. *International Journal of Speleology* **44**, 1.
- Frisia, S., Badertscher, S., Borsato, A., Susini, J., Göktürk, O.M., Cheng, H., Edwards, R.L., Kramers, J., Tüysüz, O., Fleitmann, D., 2008. The use of stalagmite geochemistry to detect past volcanic eruptions and their environmental impacts. *PAGES News* **16**, 25–26.
- Frisia, S., Borsato, A., Fairchild, I.J., Susini, J., 2005. Variations in atmospheric sulphate recorded in stalagmites by synchrotron micro-XRF and XANES analyses. *Earth and Planetary Science Letters* **235**, 729–740.
- Frumkin, A., Stein, M., 2004. The Sahara–East Mediterranean dust and climate connection revealed by strontium and uranium isotopes in a Jerusalem speleothem. *Earth and Planetary Science Letters* **217**, 451–464.

- Gao, C., Robock, A., Ammann, C., 2008. Volcanic forcing of climate over the past 1500 years: an improved ice core-based index for climate models. *Journal of Geophysical Research* **113**, D23111.
- Gázquez, F., Calaforra, J.M., Forti, P., Ghaleb, B., Delgado-Huertas, A., 2014. Paleoflood events recorded by speleothems in caves. *Earth Surface and Landforms* **39**, 10, 1345–1353.
- Gibelin, A.L., Deque, M., 2003. Anthropogenic climate change over the Mediterranean region simulated by a global variable resolution model. *Climate Dynamics* **20**, 237–339.
- Ginés, J., Fornós, J., Ginés, A., Merino, A., Gràcia, F., 2014. Geologic constraints and speleogenesis of Cova des Pas de Vallgornera, a complex coastal cave from Mallorca Island (western Mediterranean). *International Journal of Speleology* **43**, 2, 105–124.
- Giorgi, F., 2006. Climate change hot-spots. *Geophysical Research Letters* **33**. doi:10.1029/2006GL025734.
- Giorgi, F., Lionello, P., 2008. Climate change projections for the Mediterranean region. *Global and Planetary Change* **63**, 90–104.
- González-Lemos, S., Müller, W., Pisonero, J., Cheng, H., Edwards, R.L., Stoll, H.M., 2015. Holocene flood frequency reconstruction from speleothems in northern Spain. *Quaternary Science Reviews* **127**, 129–140. <https://doi.org/10.1016/j.quascirev.2015.06.002>.
- Goudie, A.S., Middleton, N.J., 2001. Saharan dust storms: nature and consequences. *Earth-Science Reviews* **56**, 179e204.
- Grimalt, M., Rosselló, J., 2018. Traditional flood mitigation measures in Mallorca. In: Antronico, L., Marincioni, F. (Eds.), *Natural Hazards and Disaster Risk Reduction Policies*. Geographies of the Anthropocene. II Sileno Edizioni, Lago, Italy, pp. 243–260.
- Grimalt-Gelabert, M., Bauzá-Llinàs, J., Genovart-Rapado, M.C., 2021. The flood of October 9, 2018 in the city centre of Sant Llorenç des Cardassar (Mallorca). *Cuadernos de Investigación Geográfica* **47**, 265–286.
- Grimalt-Gelabert, M., Rosselló-Geli, J., Bauzá-Llinàs, J., 2020. Flood related mortality in a touristic island: Mallorca (Balearic Island) 1960–2018. *Journal of Flood Risk Management* **13**, e12644.
- Hodge, E.J., 2004. Palaeoclimate of the Western Mediterranean Region: Results From Speleothems. Unpublished PhD thesis, University of Bristol, Bristol.
- Hodge, E.J., Richards, D.A., Smart, P.L., Ginés, A., Mattey, D.P., 2008. Sub-millennial climate shifts in the western Mediterranean during the last glacial period recorded in a speleothem from Mallorca, Spain. *Journal of Quaternary Science* **23**, 713–718.
- Homar, V., Ramis, C., Romero, R., Alonso, S., 2010. Recent trends in temperature and precipitation over the Balearic Islands (Spain). *Climatic Change* **98**, 199–211.
- Jansen, J.H.F., Van der Gaast, S.J., Koster, B., Vaars, A.J., 1998. CORTEX, a shipboard XRF-scanner for element analyses in split sediment cores. *Marine Geology* **151**, 143–153.
- Lionello, P., Malanotte-Rizzoli, P., Boscolo, R., 2006. *Mediterranean Climate Variability*. Elsevier, Amsterdam.
- Lionello, P., Sanna, A., 2005. Mediterranean wave climate variability and its links with NAO and Indian monsoon. *Climate Dynamics* **25**, 611–623.
- Lund, D.C., Lynch-Stieglitz, J., Curry, W.B., 2006. Gulf Stream density structure and transport during the past millennium. *Nature* **444**, 601–604.
- Margaritelli, G., Cisneros, M., Cacho, I., Vallefucio, M., Rettori, R., Lirer, F., 2018. Climatic variability over the last 3000 years in the central-western Mediterranean Sea (Menorca Basin) detected by planktonic foraminifera and stable isotope records. *Global and Planetary Change* **169**, 179–187.
- Mariotti, A., Zeng, N., Yoon, J.H., Artale, V., Navarra, A., Alpert, P., Li, L.Z.X., 2008. Mediterranean water cycle changes: transition to drier 21st century conditions in observations and CMIP3 simulations. *Environmental Research Letters* **3**, 044001.
- Martín-Chivelet, J., Muñoz-García, M.B., Cruz, J.A., Ortega, A.I., Turrero, M.J., 2017. Speleothem architectural analysis: integrated approach for stalagmite-based paleoclimate research. *Sedimentary Geology* **353**, 28–45.
- Martínez-Martínez, J., Fusi, N., Barberini, V., Cañaveras, J.C., Crosta, G.B., 2010. X-Ray Microtomography for studying 3D-textures of speleothems developed inside historic walls. *Revista de la Sociedad Española de Mineralogía* **13**.
- Martínez-Pillado, V.I., Iriarte, Y.E., Álvaro, A., Ortega, N., Aranburu, A., Arsuaga, J.L., 2020. The red coloration of Goikoetxe Cave's speleothems (Busturia, Spain): an indicator of paleoclimatic changes. *Quaternary International* **566–567**, 141–151.
- Martín-Puertas, C., Jiménez-Espejo, F., Martínez-Ruiz, F., Nieto-Moreno, V., Rodrigo, M., Mata, M.P., Valero-Garcés, B.L., 2010. Late Holocene climate variability in the southwestern Mediterranean region: an integrated marine and terrestrial geochemical approach. *Climate of the Past* **6**, 807–816.
- Mayewski, P.A., Maasch, K., Yan, Y., Kang, S., Meyerson, E., Sneed, S., Kaspari, S., et al., 2006. Solar forcing of the polar atmosphere. *Annals of Glaciology* **41**, 147–154.
- McGregor, H.V., Evans, M.N., Goosse, H., Leduc, G., Martrat, B., Addison, J.A., Mortyn, P.G., et al., 2015. Robust global ocean cooling trend for the pre-industrial Common Era. *Nature Geoscience* **8**, 671–677.
- Mees, F., Swennen, R., Van Geet, M., Jacobs, P., 2003. *Applications of X-Ray Computed Tomography in the Geosciences*. Geological Society, London.
- Mickler, P.J., Ketcham, R.A., Colbert, M.W., Banner, J.L., 2004. Application of high-resolution X-ray computed tomography in determining the suitability of speleothems for use in paleoclimatic, paleohydrologic reconstructions. *Journal of Cave and Karst Studies* **66**, 4–8.
- Miller, G.H., Geirsdóttir, Á., Zhong, Y., Larsen, D.J., Otto-Bliesner, B.L., Holland, M.M., Bailey, D.A., et al., 2012. Abrupt onset of the Little Ice Age triggered by volcanism and sustained by sea-ice/ocean feedbacks. *Geophysical Research Letters* **39**, L02708.
- Mix, A.C., Rugh, W., Pisias, N.G., Veirs, S., 1992. Leg 138 Shipboard Sedimentologists (Hagelberg, T., Hovan, S., Kemp, a., Leinen, M., Levitan, M., Ravelo, C.), the Leg 138 Scientific Party, 1992. *Color reflectance spectroscopy: a tool for rapid characterization of deep-sea sediments. Paper presented at the Proceedings of the Ocean Drilling Program. Part A, Initial Report* **138**, 67–77. http://www.coas.oregonstate.edu/facultypages/Mix/Mix_et_al_1992_ODP138ir_color.pdf.
- Morellón, M., Valero-Garcés, B., González-Sampériz, P., Vegas-Vilarrúbia, T., Rubio, E., Rieradevall, M., Delgado-Huertas, et al., 2011. Climate changes and human activities recorded in the sediments of lake Estanya (NE Spain) during the Medieval warm period and little Ice age. *Journal of Paleolimnology* **46**, 423–452.
- Moreno, A., Cacho, I., Canals, M., Gromalt, J.O., Sanchez-Vidal, A., 2004. Millennial-scale variability in the productivity signal from the Alboran Sea record, Western Mediterranean Sea. *Palaeogeography, Palaeoclimatology, Palaeoecology* **211**, 205–219.
- Moreno, A., Cacho, I., Canals, M., Prins, M.A., Sánchez-Goñi, M.F., Grimalt, J.O., Weltje, G.J., 2002. Saharan dust transport and high latitude glacial climatic variability: the Alboran Sea record. *Quaternary Research* **58**, 318–328.
- Moreno, A., Valero-Garcés, B.L., González-Sampériz, P., Rico, M., 2008. Flood response to rainfall variability during the last 2000 years inferred from the Taravilla Lake record (Central Iberian Range, Spain). *Journal of Paleolimnology* **40**, 943–961.
- Muhs, D.R., Budahn, J., Avila, A., Skipp, G., Freeman, J., Patterson, D., 2010. The role of African dust in the formation of Quaternary soils on Mallorca, Spain and implications for the genesis of Red Mediterranean soils. *Quaternary Science Reviews* **29**, 2518–2540.
- Muñoz, A., Bartolomé, M., Muñoz, A., Sancho, C., Moreno, A., Hellstrom, M.C.J., Osácar, C.M., Cacho, I., 2015. Solar influence and hydrological variability during the Holocene from a speleothem annual record (Molinos Cave, NE Spain). *Terra Nova* **27**, 300–311.
- Muñoz-García, M.B., Cruz, J., Martín-Chivelet, J., Ortega, A.I., Turrero, M.J., López-Elorza, M., 2016. Comparison of speleothem fabrics and micro-stratigraphic stacking patterns in calcite stalagmites as indicators of paleoenvironmental change. *Quaternary International* **407**, 74–85.
- Nederbragt, A.J., Thurow, J., 2004. Digital sediment colour analysis as a method to obtain high resolution climate proxy records. In: Francus, P. (Ed.), *Image Analysis, Sediments and Palaeoenvironments*. Kluwer Academic, Dordrecht, Netherlands, pp. 105–124.
- Nieto-Moreno, V., Martínez-Ruiz, F., Giralt, S., Jiménez-Espejo, F., Gallego-Torres, D., Rodrigo-Gámiz, M., García-Orellana, J., Ortega-Huertas, M., de Lange, G. J., 2011. Tracking climate variability

- in the western Mediterranean during the Late Holocene: a multiproxy approach. *Climate of the Past* 7, 1395–1414.
- Parnell, A.C., Haslett, J., Allen, J.R.M., Buck, C.E., Huntley, B.**, 2008. A flexible approach to assessing synchronicity of past events using Bayesian reconstructions of sedimentation history. *Quaternary Science Reviews* 27, 1872–1885.
- Pastor, F., Estrela, M.J., Peñarrocha, D., Millán, M.M.**, 2001. Torrential rains on the Spanish Mediterranean coast: modelling the effects of the sea surface temperature. *Journal of Applied Meteorology* 40, 1180–1195.
- Pino, D., Alberola, A., Balasch, J.C., Barriendos, M., Gil, S., Grau-Satorras, M., Mazón, J., Pérez Morales, A., Tuset, J.**, 2018. Major flood events reconstruction from a multi-proxy approach. The case study of November 1617 flood event in the Mediterranean Basins of Iberian Peninsula. *Geophysical Research Abstracts* 20, EGU2018-10386.
- Polyak, V.P., Onac, B.P., Fornós, J.J., Hay, C., Asmeron, Y., Dorale, J.A., Ginés, J., Tuccimei, P., Ginés, A.**, 2018. A highly resolved record of relative sea level in the western Mediterranean Sea during the last interglacial period. *Nature Geoscience* 11, 860–864.
- Ramos-Román, M.J., Jiménez-Moreno, G., Camuera, J., García-Alix, A., Anderson, R.S., Jiménez-Espejo, F.J., Carrión, J.S.**, 2018. Holocene climate aridification trend and human impact interrupted by millennial- and centennial-scale climate fluctuations from a new sedimentary record from Padul (Sierra Nevada, southern Iberia Peninsula). *Climate of the Past* 14, 117–137.
- Robock, A.**, 2000. Volcanic eruptions and climate. *Reviews of Geophysics* 38, 191–219.
- Rodrigo-Gámiz, M., Martínez-Ruiz, F., Jiménez-Espejo, F.J., Gallego-Torres, D., Nieto-Moreno, V., Romero, O., Ariztegui, D.**, 2011. Impact of climate variability in the western Mediterranean during the last 20,000 years: oceanic and atmospheric responses. *Quaternary Science Reviews* 30, 2018–2034.
- Rogerson, M., Weaver, P.P.E., Rohling, E.J., Lourens, L.J., Murray, J.W., Hayes, A.**, 2006. Color logging as a tool in high-resolution paleoceanography. In: Rothwell, R.G. (Ed.), *New Techniques in Sediment Core Analysis*. Geological Society of London Special Publication 267, 99–112.
- Rothwell, R.G., Rack, F.R.**, 2006. New techniques in sediment core analysis: an introduction. In: Rothwell, L.G. (ed.), *New Techniques in Sediment Core Analysis*. Geological Society of London Special Publication 267, 1–29.
- Sheffield, J., Wood, E.F.**, 2008. Projected changes in drought occurrence under future global warming from multi-model, multi scenario, IPCC AR4 simulations. *Climate Dynamics* 31, 79–105.
- Thorndycraft, V.R., Barriendos, M., Benito, G., Rico, M., Casas, A.**, 2006. The catastrophic floods of AD 1617 in Catalonia (northeast Spain) and their climatic context. *Hydrological Sciences Journal* 51, 5, 899–912.
- Torner, J., Cacho, I., Moreno, A., Sierro, F.J., Martrat, B., Rodríguez-Lazaro, J., Frigola, J., et al.**, 2019. Ocean–atmosphere interconnections from the last interglacial to the early glacial: an integration of marine and cave records in the Iberian region. *Quaternary Science Reviews* 226, 106037.
- Tsimplis, M.N., Josey, S.A.**, 2001. Forcing of the Mediterranean Sea by atmospheric oscillations over the North Atlantic. *Geophysical Research Letters* 28, 803–806.
- Ulbrich, U., May, W., Li, L., Lionello, P., Pinto, J. G., Somot, S.**, 2006. The Mediterranean climate change under global warming. In: Lionello, P., Malanotte-Rizzoli, P., Boscolo, R. (Eds.), *Mediterranean Climate Variability*. Elsevier, Amsterdam, pp. 398–415.
- Vanghi, V., Iriarte, E., Aranburu, A.**, 2015. High resolution X-ray computed tomography for petrological characterization of speleothems. *Journal of Cave and Karst Studies* 77, 75–82.
- Vansteenberghe, S., Winter, N.J., Sinnesael, M., Xueqin, Z., Verheyden, S., Claeys, P.**, 2020. Benchtop μ XRF as a tool for speleothem trace elemental analysis: Validation, limitations and application on an Eemian to early Weichselian (125–97 ka) stalagmite from Belgium. *Palaeogeography, Palaeoclimatology, Palaeoecology* 538, 109460.
- Vesica, P.L., Tuccimei, P., Turi, B., Fornós, J.J., Ginés, A., Ginés, J.**, 2001. Late Pleistocene Paleoclimates and sea-level change in the Mediterranean as inferred from stable isotope and U-series studies of overgrowths on speleothems, Mallorca, Spain. *Quaternary Science Reviews* 19, 865–879.
- Walczak, I.W., Baldini, J.L., Baldini, L.M., McDermott, F., Marsden, S., Standish, C.D., Richards, D.A., Andreo, B.**, 2015. Reconstructing high-resolution climate using CT scanning of unsectioned stalagmites: a case study identifying the mid-Holocene onset of the Mediterranean climate in southern Iberia. *Quaternary Science Reviews* 127, 117–128.
- Westland, S.**, 2012. *Frequently Asked Questions About Colour Physics*. Kindle Edition.
- Zisu, N.S., Schwarcz, H.P., Konyer, N., Chow, T., Noseworthy, M.D.**, 2012. Macroholes in stalagmites and the search for lost water. *Journal of Geophysical Research: Earth Surface* 117. doi:10.1029/2011JF002288.